





Effect of double quantum dot asymmetry on electron localization

Igor Filikhin ^{*,§}, Abdennaceur Karoui ^{*}, Tanja Zatezalo^{*}, Sergei P. Kruchinin ^{†,‡,¶} and
Branislav Vlahovic ^{*}

**CREST/Mathematics and Physics Department,
North Carolina Central University,
Durham, NC 27707, USA*

*†Bogolyubov Institute for Theoretical Physics, NASU,
Metrologichna Street 14-b, 03143 Kiev, Ukraine*

*‡Felix Bloch Institute for Solid State Physics,
University of Leipzig, Linnestr. 5, 04103, Leipzig, Germany*

§ifilikhin@nccu.edu

¶sergeikruchinin@yahoo.com

Received 9 October 2023

Accepted 12 October 2023

Published 30 November 2023

In this paper, we study the localization of an electron in a binary quantum system formed by a pair of quantum dots (QDs). The traditional theoretical consideration of such systems is limited to the symmetrical case when QDs in such double quantum dot (DQD) are assumed identical in all respects. In this paper, we model the effects of breaking QD similarities in a DQD by studying two-dimensional (2D) DQDs as a double quantum well (DQW). This is done by solving the Schrödinger equation, with parameters chosen to describe an InAs/GaAs heterostructure. We calculate the energy spectrum of the electron confinement and the spectral distribution of localized/delocalized spatial states. Both symmetric and asymmetric QW shapes are considered and their effects are compared. The effects of symmetry breaking are explained within the framework of the two-level system theory. We delineate the QW weak and strong coupling cases in DQW. In particular, we show that the coherence in ideal DQW is unstable in the case of a weak QW coupling. Within the framework of the proposed approach, a charge qubit realized on a DQD is discussed and, as an example, a qubit based on an almost ideal DQD is proposed.

Keywords: Electron tunneling; electron localization; quantum wells; semiconductors; charge qubit.

1. Introduction

The goal of this paper is to explore the significance of symmetry breaking on the stability of tunneling in binary quantum system, like quantum dots (QDs) or (QWs). The importance of such systems is due to their relevance to building quantum computers.¹ One of the main concepts employed for quantum computer design is the

§Corresponding author.

spatial isolation of single electron in a double quantum dot (DQD).^{2–6} Charge qubit based on electron localization in the left or right QD of a DQD has been reported in Refs. 7–10. One of the main problems with quantum computing is the induction of qubit errors. This issue seems to be inevitable, since quantum states of qubits are sensitive to slight variations of temperature, tiny vibration, or stray photons, even single photon. These can cause random change of the qubit state, which gives non-controllable error. The state of neighboring qubits can also change haphazardly as a QD can couple to signals captured by their neighbors. The quantum fluctuations or charge noise on a controlled phase gate may perturb the charge stability in a substantial way.^{9,11,13,14} Understanding the symmetry breaking issues has a crucial applicability in quantum engineering since it instructs on the way quantum states of QDs¹⁵ coupling is utilized. Moreover, such understanding lays the ground for advanced manufacturing of next generation device fabrication and quantum devices.

We have recently proposed an approach to studying electron tunneling in a DQD based on modeling the spatial distribution of a single electron in the DQD for the energy levels of the entire spectrum. The theoretical description for electron states in InAs/GaAs heterostructures is based on the effective potential model proposed in Ref. 16. Main aspects of symmetry violation and how each affects the entanglement were studied and reported in Refs. 17–20. In line with this study, we here-in evaluate how small variations of the system geometrical parameters (QD size and shape, and the DQD topology) and the applied fields will affect the stability of localized/delocalized states in DQD. Also, we delineate the limits at which charge tunneling in ideal DQD becomes unstable with due to small fluctuations affecting across the whole spectrum of the electron confinement spectrum. We argue that the QD coupling in an ideal DQD (initially defined as a system with infinite coherence) can become unstable for any small fluctuations, Δ , in the energy of electron levels. This feature turns the DQD into an extremely sensitive sensor; as suggested in our paper.¹⁷

In this paper, we focus on two types of charge qubit effectors: (i) the medium, which distorts the wave function of an electron in coupled DQD, and (ii) the quantum state fluctuations (like an electrical pulse variations) induce an asymmetry. Fluctuation risers (for instance, a molecule that is being detected, or pressure that strains the device, or a tiny displacement in the range of atomic bond length) change the coupling parameter W and asymmetry Δ of bi-confinement in DQD. Our numerical modeling aims at analyzing the dynamics of localized/delocalized states in electron spectrum under DQD geometry variations. We demonstrate that the ratio W/Δ determines the electron localization within the DQD. The modeling of the variations of the geometry allows us to simulate the effects of environmental influence and asymmetry fluctuations on the coherence in the DQD based charge qubit. We show that the numerical uncertainty like 0/0 takes place due to the ratio W/Δ and defines the spectral distribution of localized/delocalized states in ideal DQD ($\Delta = 0$). Such an ideal system is suitable as a model for a theoretical description of quantum systems for only the limiting case where the mathematical limit $\Delta \rightarrow 0$

is possible. In this paper, we consider realistic binary quantum systems, which are usually asymmetric ($\Delta > 0$).

Our theoretical model of InAs/GaAs heterostructures for QDs is presented in Sec. 2 of this paper. In Sec. 3, theoretical discussion of two-level systems, anti-crossing levels, and electron coupling in double quantum dots (DQDs) is given. The notations for describing the electron localization in DQD are presented in Sec. 4. To illustrate the theory assumptions, the results of our calculations for the electron tunneling in symmetrical and asymmetrical DQWs are presented in Sec. 5. Here, we discuss numerical examples of distributions of localized and delocalized states in the spectrum of a single electron. The numerical impacts and the influence of geometry factors on the tunneling for two cases, the ideal and non-ideal symmetric DQW are shown. Interpretation of the results is presented in Sec. 6. We describe the spectral instability of charge carrier tunneling in DQD in relation to the effects of environmental influence (e.g. fluctuations of electrical pulse) on the coherence of DQD based charge qubit. A number of lasting statements on these quantum effects are provided.

2. Effective Model for InAs/GaAs Quantum Dots

The electron state in InAs/GaAs QDs is modeled¹⁶ based on the kp -perturbation in the framework of the single sub-band effective mass approximation. In this case, the eigenvalue problem is formulated by the Schrödinger equation

$$(\hat{H}_{kp} + V_c(r) + V_s(r))\Psi(r) = E\Psi(r), \quad (1)$$

where E is the electron binding energy, \hat{H}_{kp} is the single band kp -Hamiltonian operator $\hat{H}_{kp} = -\nabla \frac{\hbar^2}{2m^*} \nabla$, m^* is the electron effective mass, which depends on the electron coordinates written as $m^*(r)$, and $V_c(r)$ is the band gap potential. The Ben-Daniel-Duke boundary conditions²¹ are used at the QW substrate interface. Here, we describe the confinement model proposed in Ref. 16 for the conduction band. Both potentials $V_c(r)$ and $V_s(r)$ act within the QWs extent. While the potential V_c is attractive, the potential V_s is repulsive. The V_s potential reduces the strength of the electron confinement; it is added to simulate the strain effect in the InAs/GaAs heterostructure. Schematics one-dimensional (1D) representation for this band gap model is given in Fig. 1. The boundary of a two-dimensional (2D) InAs QW embedded into the GaAs substrate is shown, which embodies the spatial extents of the band gap model.

The energy barrier is such that inside the QD, the bulk conduction band offset is null, i.e. $V_c = 0$, while it is equal to $V_c > 0$ outside the QD. The band gap potential for the conduction band is fixed to $V_c(r) = 0.594$ eV. The bulk effective masses of InAs and GaAs are $m_1^* = 0.024 m_0$ and $m_2^* = 0.067 m_0$, respectively, where m_0 is the free electron mass.

The magnitude of the effective potential $V_s(r)$ that simulates the strain effect is adjusted so to reproduce experimental data for InAs/GaAs QDs. The adjustment involves the materials composing the heterojunction, and to a lesser extent, the QD topology.

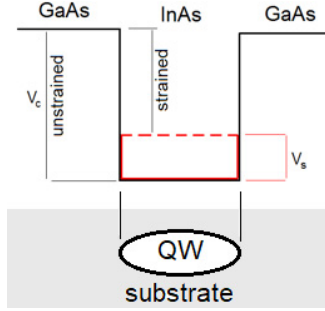


Fig. 1. (Color online) The ellipsoidal-shaped QW: the band gap model for InAs/GaAs heterojunction and geometry QW.

For example, the obtained magnitude of 0.21 eV of V_s for the conduction band was discussed in Ref. 16. This value was reconfirmed by similar results obtained from eighth band kp -calculations for InAs/GaAs QDs.²² Another value of 0.31 eV for V_s was obtained²³ from experimental data reported by Lorke *et al.*²⁴ The main advantage of using the effective potential is the theoretical simplicity, as well as the practical calculations, even in the case of complex geometry of nano-sized systems. The effective potential model is compatible²⁵ with the existing experimental data for InAs/GaAs heterostructures.²⁶

3. DQD as a Two-Level System

Let two coupled InAs/GaAs QDs be an example of a two-level system. The confinement of an electron is modeled by the 1D formalism, which can be found in Ref. 27. The electron wave function in such quantum system is represented as a superposition of two functions. The first one $|0\rangle$ is associated to an electron state of the left QD, considered as isolated. The second one $|1\rangle$ describes an electron state in right QD, considered as isolated. The superposition is represented as linear combination: $a|0\rangle + b|1\rangle$, where $|a|^2 + |b|^2 = 1$. The electron is delocalized over the DQD in this state. We describe a localized state by the condition, where a (or b) is close to zero and b (or a) is close to one.

In the $(|0\rangle, |1\rangle)$ basis, the Hamiltonian (1) takes the matrix form

$$H = \begin{pmatrix} E_+ & W_{01} \\ W_{10} & E_- \end{pmatrix}, \quad (2)$$

where W_{01} and W_{10} are the coupling matrix elements, and E_+ and E_- are energies of the electron in the coupled DQD. Note that this matrix form corresponds to the simple case of almost identical confinements in the DQD: $V_0 \approx V_1$, where V_0 (and V_1) is the confinement potential in the left (right) QD. The coupling parameter W is defined as follows:

$$W \approx W_{01} = \langle 0|V_0|1\rangle \approx W_{10} = \langle 1|V_1|0\rangle, \quad (3)$$

where V_0 and V_1 are the confinement potentials in the QWs. Thus, the coupling W expresses to overlapping wave functions of the undisturbed state of two separated QDs. In the absence of the tunnel coupling, that is when $W = 0$, the electron can be located in one or another dot with the energies E_1 and E_2 corresponding to the undisturbed states. The Hamiltonian takes the following form:

$$H = \begin{pmatrix} E_0 & 0 \\ 0 & E_1 \end{pmatrix}.$$

The corresponding Schrödinger equations reads

$$(H_0 + V_1)|0\rangle = E_0|0\rangle, \quad (H_0 + V_1)|1\rangle = E_1|1\rangle,$$

where H_0 is the operator kinetic energy of free electron: $-\nabla(\hbar^2/2m^*)\nabla$ and m^* is electron effective mass.

By diagonalizing the matrix (2), the electron single-particle energies are calculated²⁷ as

$$E_+, E_- = \frac{(E_0 + E_1) \pm \sqrt{(E_0 - E_1)^2 + 4W^2}}{2}. \quad (4)$$

When the energy difference $\Delta = |E_0 - E_1|$ is large and $\Delta \ll W$, no tunneling occurs. The minimal value for energy splitting ε between coupled states having energies E_+ and E_- occurs for the value $\Delta = 0$ when $\varepsilon = E_+ - E_- = 2|W|$. At the same time, this value of Δ corresponds to maximal energy difference between E_+ and E_0 (E_- and E_1).

The case $\Delta = 0$ could correspond to identical QDs within the DQD. In Fig. 2, the diagram plotted in (E, Δ) coordinates helps to understand this setting. This diagram presents the coupling between of two energy levels as an anti-crossing of levels. When the coupling is absent, the levels are crossed, as shown by dashed lines in Fig. 2. One can see that, for large Δ , the energies E_+ and E_- become equal to E_0 and E_1 . Analysis of Eq. (4) gives the same result.

4. Electron Localization in Double Quantum Wells

In this section, we present the formalism that allowed us to analyze the electron localization and spectral distributions of localized/delocalized states in DQWs

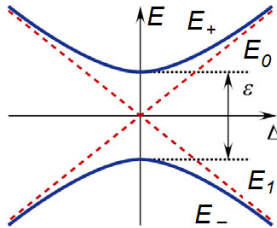


Fig. 2. (Color online) The anti-crossing in a two-level system as dependence of the energy of levels, E_+ , E_- , (solid curves) on the difference Δ of energies E_1 and E_0 , of the corresponding levels for uncoupled system (red dashed lines).

and dots. Note that an experimental detection of the excited states in DQD has been proposed in Ref. 28, the authors used capacitive charge sensing to single out such states. It was shown in Ref. 17 that the spectral distributions of localized/delocalized states are extremely sensitive to the breaking of the DQD shape symmetry. To explain this statement, we consider electron levels in 1D bi-confinement potential with the energies $E^{(n)}$, $n = 1, 2, 3 \dots$ listed in increased order of energy values. The model utilizes the coupling parameter, Θ , which defines the delocalized ($\Theta \approx \frac{\pi}{2}$) and localized ($\Theta \approx 0$) states of a single electron. This parameter depends on $\Delta^{(n)}$, the difference between energy levels of the left and right DQWs, the considered spectra are those of separated QWs. In this study, the difference is caused by a shape symmetry breaking. For 1D two-level system, the dependence of the localization of a single electron in DQW may be expressed²⁷ by the ratio $W^{(n)}/\Delta^{(n)}$, where W^n is defined by the wave functions overlaps for separated QWs and $\Delta^{(n)}$ is the energy difference between n th electron levels in the spectra of separated QWs:

$$\Theta^{(n)} = \arctan(2W^{(n)}/\Delta^{(n)}), \quad n = 1, 2, 3, \dots \quad (5)$$

The dependence of Θ on the ratio $2W/\Delta$ is shown in Fig. 3. Here, the delocalized state corresponds to a coupling in the QWs. The wave functions of each levels (the spectral quasi-doublet, defined in Eq. (4)) can be expressed as follows:

$$|+\rangle = |0\rangle + \tan(\Theta/2)|1\rangle, \quad |-\rangle = -\tan(\Theta/2)|0\rangle + |1\rangle, \quad (6)$$

where the normalizing constant is arbitrary. The wave functions of the unperturbed states are noted for ψ_1 and ψ_2 and indexed by 1 or 2 for separated left and right quantum wells, respectively. For identical QWs in DQW, each unperturbed energy level splits to two according to Eq. (4), where $E_0 = E_1$. To analyze the electron localization, we calculate the single electron average coordinate $\langle x \rangle$, calculated as matrix elements

$$\langle x \rangle_i = \langle i|x|i\rangle, \quad \langle x \rangle_{ij} = \langle i|x|j\rangle, \quad i, j = 0, 1,$$

which are associated, respectively, with the electron wave functions $|i\rangle$ in QW₁ and QW₂, considered separate. The x -coordinate origin is chosen to be the mid-point of

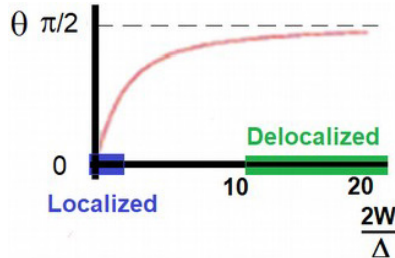


Fig. 3. (Color online) The localization of single electron in DQW: the relation between the coupling parameter Θ and the ratio $2W/\Delta$ for a confinement level in DQW is given. We show the ranges for localized and delocalized states of the electron by blue and green highlighting.

the two QWs. The average coordinates $\langle x \rangle_+$ and $\langle x \rangle_-$ can be written as

$$\langle x \rangle_+ = \langle x \rangle_0 + \tan^2(\Theta/2)\langle x \rangle_1 + 2 \tan(\Theta/2)\langle x \rangle_{01} \quad (7)$$

and

$$\langle x \rangle_- = \tan^2(\Theta/2)\langle x \rangle_0 + \langle x \rangle_1 - 2 \tan(\Theta/2)\langle x \rangle_{10}, \quad (8)$$

for the corresponding quasi-doublets within the electron spectrum. Single electron can be localized in one or another QW and $\langle x \rangle_+ \approx \langle x \rangle_0$ and $\langle x \rangle_- \approx \langle x \rangle_1$.

The sensitivity of the coupling parameter Θ to small variations of Δ and W is estimated¹⁷ as

$$\delta(\Theta) \sim -\frac{W}{\Delta^2 + 4W^2} \delta(\Delta) + \frac{2\Delta}{\Delta^2 + 4W^2} \delta(W), \quad (9)$$

where W and Δ are selected from W_n and Δ_n , they depend on the quantum numbers n .

5. 2D DQD: Electron Localization and DQD Geometry

The numerical analysis discussed in this section concerns electron tunneling in a typical InAs/GaAs DQW. Such a DQW is modeled using the material and geometric parameters considered above and taking into account either identical QWs (ideal DQWs) or nearly ideal DQWs (formed by knowingly non-identical QWs). These two types of DQW geometries differ significantly¹⁷; small variations of the ideal DQW geometry that break the symmetry drastically distort the spectral distribution of tunnel states. Our choice of DQD geometry is motivated by the experimental results of fabricated DQDs described in Ref. 29, where QD pairs are made mostly ellipsoidal.

In the ideal DQW, the probability for an electron to be in the left QW or in the right one is, according to Eq. (6), equal to 1/2 for all confinement states of the DQW. This tunneled state corresponds to the limits $\Delta \rightarrow 0$, finite W value, and the relation $W > \Delta$. This occurs when $\Theta \sim \pi/2$ and $\tan(\Theta/2) \sim 1$. The relation (6) takes the following form of symmetric and anti-symmetric configurations:

$$|+\rangle = |0\rangle + |1\rangle, \quad |-\rangle = -|0\rangle + |1\rangle.$$

Normalization leads to writing the electron probability as

$$\langle \pm | \pm \rangle = \langle 0|0\rangle/2 + \langle 1|1\rangle/2,$$

due to orthogonality of the elements of the basis $\langle 0|1\rangle = \langle 1|0\rangle = 0$.

The condition $\Delta \rightarrow 0$ relates to the degree of QW similarity within the DQD system. By realizing this limit, the condition $W > \Delta$ holds for any small value W . It mathematically means that there is not a limit for inter-dot distance for which the coherence is lost. Ideally, the wave function of the separated QW is spread everywhere and one can always find nonzero W values. Thus, the ratio $2W/\Delta$ always goes to infinity when $\Delta \rightarrow 0$. The latter means that the delocalized (coherent) state does not depend on inter-dot distance in an ideal DQD (see Fig. 3). Obviously, a realistic consideration does not agree with such ideal model.

The limit $\Delta \rightarrow 0$ is a mathematical idealization, for which the spectral distribution of delocalized states corresponds to maximal coherence in the ideal DQW. However, the ideal system is unstable relatively to small fluctuations. This conclusion flows down from the results of our calculations, where the numerical approximation errors simulate small variations of the parameter Δ of the almost ideal DQD. The calculated values include the electron confinement energy and wave function which are obtained by solving numerically the Schrödinger equation (1). We use the averaged x -coordinate of electron to definite localization in the DQW according to Eqs. (7) and (8). The spectral distribution of localized and delocalized states for symmetric DQW is shown Fig. 4(a). For these calculations, we used the DQW geometry shown in Fig. 1, where both QW1 and QW2 are perfect ellipses with semi-axes $R_x = 55$ nm and $R_y = 35$ nm and with inter-dot distance $a = 5$ nm. In Fig. 4(a), the localized/delocalized states are shown for three different meshes chosen for the finite element analysis (FEA). The mesh sizes were chosen to be fine and up to the full extent of the available computer memory (32 GB) and to the limit of software capabilities in terms of handing meshing nodes. Practically, the meshes lead inevitably to different geometries for the DQW as well as for each QWs due to finite element approximation for the geometry being studied. The calculations for the largest mesh (Mesh 1) demonstrate domination of the localized states in the spectrum (black dots). The finest mesh (Mesh 2) appeared to provide larger delocalizing (red open circles). The energy spectrum of single electron can be sorted according to

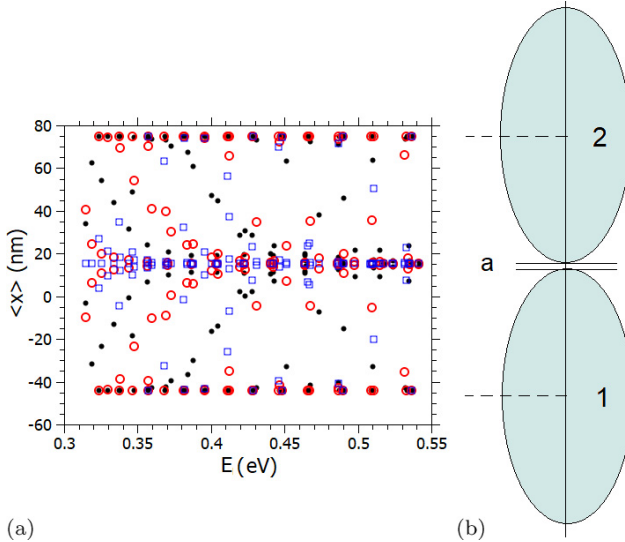


Fig. 4. (Color online) (a) The ideal DQW: the tunneling in symmetric ellipsoidal DQW: the sizes of the QW₁ and QW₂ are equal. The results of calculation for different three meshes are shown by dots (Fine mesh), open circles (Finer mesh), and open rectangles (Finest mesh). (b) Schematic deposition of the QWs in the DQW with relation to the averaged coordinate $\langle x \rangle$ of the localized states (dashed lines). The inter-dot distance a is shown.

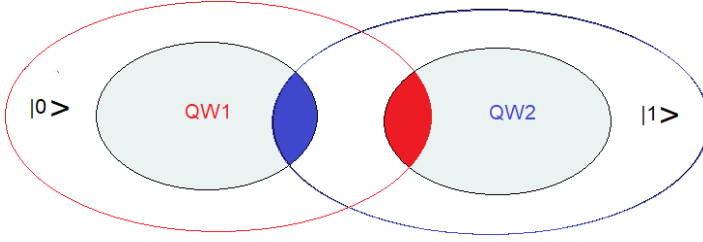


Fig. 5. (Color online) The schematic representation of the QWs (QW1 and QW2, in light blue areas) that are separated (without a coupling). The extent of the electron wave function for ground states is shown by blue and red circles. The integration in Eq. (3) for W is performed over these circles. The areas of overlapping (blue and red colors) formed by the confinement potentials (V_0 and V_1) and the functions $|0\rangle$ and $|1\rangle$ give an essential contribution to the integrals (3).

electron localization probability. As a result, a set of localized states (in the left QW or right QW) appears either at around $\max \langle x \rangle$ and $\min \langle x \rangle$, or around $\langle x \rangle \sim 75$ and -45 nm, where states have different probabilities of being in the left and right QWs. The results obtained using Mesh 3 (purple dots) are essentially clustered around $\langle x \rangle = 15$ nm indicating that delocalized states become dominating. The finalized result can be obtained by the smallest possible mesh cell size, such decrease is numerically limited inherent to the finite elements methods and computing capability.

To interpret this numerical result, one must examine the coupling W with more details. In Fig. 5, the graphical representation for Eq. (3) shows the regions of the integration for the electron wave functions of the ground state. The result of the integration depends on the overlapping of the wave functions of separated QWs. The parameters that define this overlapping are the distance between QWs and the single wave function spillover outside the QW spatial extent. The spillover is energy level dependent. The wave function spread is due to the asymptotic behavior of the confined states; such asymptotic behavior is written as

$$\Psi(x) \sim A \exp(-b\sqrt{E_c - E}x), \quad (10)$$

where x is the distance from a QW boundary, A and b are constants: these would depend at most on quantum numbers (e.g. orbital numbers). Here, E_c definitely is the bottom of the quantum well. The effective orbital quantum number defines the symmetry of wave functions of the electron levels. The integration of the functions having similar symmetries leads to a similar result. It is visible in Fig. 6 for the spectral distribution of the averaged coordinate where the tracks correspond to similar symmetry of the wave functions. The coupling parameter W may depend on the configuration of the geometry in the QW. For example, ellipsoidal QWs produce smaller W value than the circular QWs as a result of the smaller integration area.

From the numerical experiment shown in Fig. 4, one can conclude that the DQW geometry asymmetry leads to weak coupling in the systems. Numerical calculations

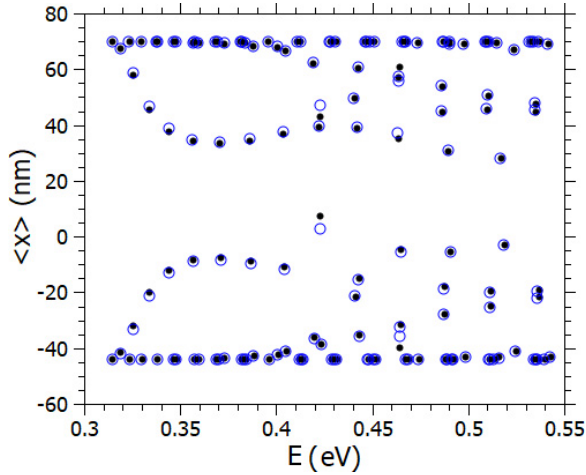


Fig. 6. (Color online) The tunneling in almost ideal DQW: asymmetric ellipsoidal dots (size of $\text{QW}_1(R_x/R_y = 55/35)$) are larger than the size of $\text{QW}_2(R_x/R_y = 55/34.75)$. The QW horizontal axes are shifted by $s = 1$ nm. Open and close circles show the results related to the variations of the solver mesh.

were unstable within the finite element approximation. The simple analysis of the interplay between the coupling parameter W and the spectra energy shift Δ given above is appropriate for this situation when the coupling in DQW is weak and W is small. Equation (9) helps us to understand the instability of such tunneling. The simple analysis taking into account that $W \leq \Delta$ and $\Delta \approx 0$ leads to the following relation:

$$\delta(\Theta) \sim \frac{W}{\Delta^2} \delta(\Delta), \quad (11)$$

which means that small variations of Δ can produce large variations of the parameter Θ that determine the electron localization as well as $\delta(\Theta) \sim \frac{1}{\Delta} \delta(\Delta)$.

To demonstrate the effect of the symmetry breaking for the electron confinement in DQW, we change the ellipsoidal geometry of the DQW, presented above to the one when the size of QW_1 with the semi-axes ratio ($R_x/R_y = 55/35$) is larger than the size of QW_2 with the ratio ($R_x/R_y = 55/34.75$). The QW horizontal axes are shifted by $s = 1$ nm. The results of the calculations for asymmetric DQW are shown in Fig. 6 where the Mesh 2 and Mesh 3 from previous calculations for ideal DQW have been used. By comparing this result and results for the ideal case, we can conclude that the asymmetric case is numerically more stable, and converges more rapidly. The effect of the mesh variations is not clearly discernable. However, in this case, the localized states dominate the spectrum. Thus, an asymmetry within the DQW plays a significant role as it hinders and even blocks the electron tunneling. For non-identical QDs in DQD, when $\Delta^{(n)} > 0$ and $W^{(n)}$ is small, the ratio (5) strongly depends on the strength the coupling $W^{(n)}$ that determines the spectral distribution of the tunneling. Generally, due to $W^{(n)}$ being small, the localized states dominate according to the

relation $W^{(n)}/\Delta^{(n)} \sim 0$. From Fig. 6, we can conclude that the spectral distribution for localization of the electron corresponds to the dependence of $W^{(n)}$ on the quantum number n numbering the spectral levels. One can separate sets of energy levels with similar tunneling strengths. These sets are formed by similar spatial distribution of the wave function, which depends on quantum numbers (e.g. radial and orbital quantum numbers). Variations in the electron localization depending on the change in the parameter W are also shown in Fig. 4. Note that here that the inter-dot distance could be the input parameter, which affects the coupling strength W more significantly. The integrals in Eq. (3) depend on the wave function overlap of separated QWs, as shown in Fig. 5. The parameters that define this overlap are the distance between QWs and the spillover of the single wave function outside of the QW shape region, which depends on the energy of the considered level and the symmetry of the wave function. The wave function spread is due to the asymptotic behavior of the confined states given by Eq. (10). The asymptotic dependence on a quantum number (e.g. orbital numbers) results in regular located traces in Figs. 4 and 6. It can be shown that the value of the logarithm of the tunneling rate $\ln(\varepsilon)$ depends on the energy as a linear function of \sqrt{E} . The tunneling rate ε is correlated to the coupling coefficient W_n . We can conclude that the contrast between ideally symmetric DQW and asymmetric one is the strong dependence of the tunneling on inter-dot (well) distance. In an ideal case, the inter-dot distance is irrelevant as it does not affect the tunneling.

Further analysis of the ellipsoidal QW considers variations of the Δ . To that end, two sets of geometry parameters are used. For the set, the semi-axis ratio R_x/R_y is considered to be 55/35 for QW1 and 55/34.90 for QW2; the relative shift s along the horizontal axis is 1 nm. The second set has the same semi-axis ratio parameters for QW1 (i.e. 33/35), but for QW2, it is chosen to be 55/34.75, while s is considered -2 nm. The first set is closest to symmetric DQW. The results of calculations are given in Fig. 7(a), wherein the first set of DQW geometry parameters corresponds to a larger degree of delocalization in the spectrum than the second DQW with a larger geometry difference.

The energy difference Δ of the spectra of the separated QWs for these two variants of DQW geometry is presented in Fig. 7(b). The tunneling is a concurrent effect of the interplay between W and Δ , both conveying the asymmetry of the two QDs. However, in this numerical experiment, the small variations Δ can affect the tunneling more significantly. The tracks which are visible in Fig. 7(a) separate the values $2W^{(n)}$ according to the spatial symmetries of corresponding wave functions. These tracks for both cases are similar. However, the values $\Delta^{(n)}$ are larger for more dissymmetrical DQW. According to Eq. (5) and Fig. 3, it means that the corresponding delocalization is weaker and states are closer to delocalization ones. One can see it in Fig. 7(a) for the low-lying energy levels, where this is clearly demonstrated. For the higher levels, this difference is mainly saved, however, increasing the values of $\Delta^{(n)}$ may be compensated by $W^{(n)}$ increasing that corresponds to a more spatially distributed wave function.

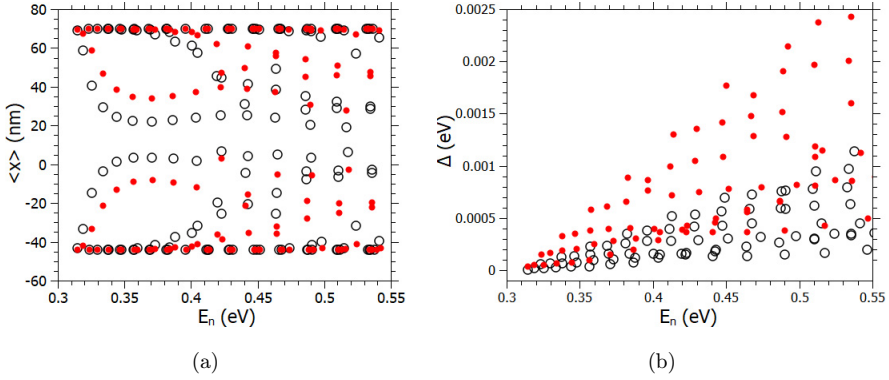


Fig. 7. (Color online) (a) The tunneling in ellipsoidal DQW with increasing asymmetry. Two set geometry parameters of the DQW were chosen. The solid circles are related to the first DQW (the set where $R_x/R_y = 55/34.75$ and $s = 1$ nm for QW2). The open circles are for the second DQW (the set where $R_x/R_y = 55/34.90$ and $s = -2$ nm for QW2). (b) The energy shift Δ of separated QW spectra for these two sets of DQW geometry.

In our next numerical experiment, we decreased the semi-axes of the ellipsoidal QWs to the values $R_x/R_y = 15/15$ for the left QW and $R_x/R_y = 15/14$ for the right QW. The change leads to increasing the coupling W . We calculate the electron localization in the lowest quasi-doublet of the spectrum for different values of the inter-dot distance a . The localization was evaluated by the averaged electron x -coordinate. The results of the calculations are shown in Fig. 8. In Fig. 8(a), the

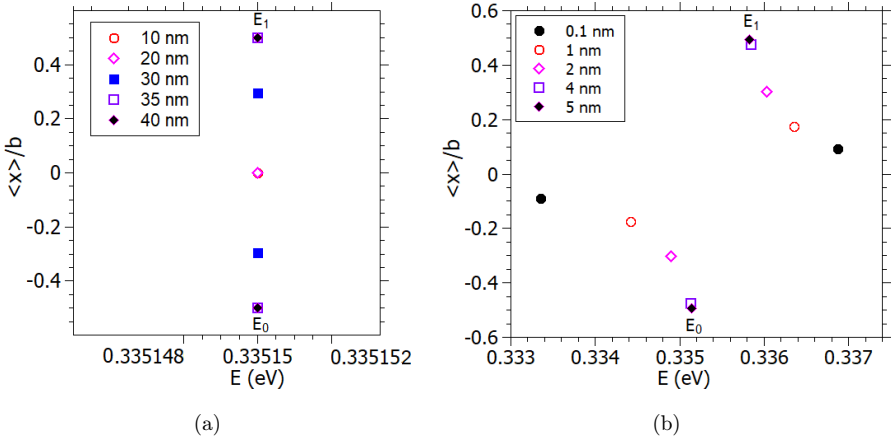


Fig. 8. (Color online) The electron localization of two lowest states of the spectrum (lowest quasi-doublet) for different values of the inter-dot distance a . The results of calculation for $\langle x \rangle/b$ are shown by different symbols. The values of a are given in the legend, b is normalizing constant: $b = a + 2R_x$. (a) The almost ideal DQW: the asymmetry of the DQW is induced by numerical FEM approximation on the finite mesh so that $\Delta < 10^{-10}$ eV. The spherical-shaped QWs have radii of 15 nm. (b) The asymmetry of the DQW is defined by the ratio $R_x/R_y = 15/14.5$ for semi-axes of the right QW. Here, the values E_0 and E_1 are pointed out to show Δ .

geometry asymmetry of the DQW is induced by numerical FEM approximation on the finite mesh so that $\Delta < 10^{-10}$ eV. We define this DQW as an almost ideal one. The ground state is a delocalized state up to $a < 20$ nm, which disagrees with previous our calculations for larger size ellipsoidal QWs with strong semi-axes deferences. In Fig. 8(b), the asymmetry of the DQW is determinate by the ratio $R_x/R_y = 15/14.5$ for semi-axes of right QW. The value for Δ can be graphically evaluated by the corresponding values E_1 and E_2 in the figure. The case of separated QWs corresponds asymptotically to the case of the largest inter-dot distance of 5 nm according to Eq. (4) for $W \sim 0$.

The significant inter-dot distance dependence of electron localization is obviously related to the high sensitivity of the matrix element W on the distance a as we have explained above. The cases of almost ideal DQW and the case of DQW with geometry-induced asymmetry are different by the values of the Δ . The smaller Δ generates a bigger value of the ratio W/Δ and provides a delocalized state of an electron for larger a .

6. 2D DQD: Modeling a Charge Qubit

Based on our approaches, we can propose an interpretation for the DQD-based charge qubit.^{7,12,30-34} We have shown in previous sections that the tunneling in a two-level system, exactly like in the DQD, is sensitive to fluctuations according to Eq. (5) and resulted by a concurrent effect of Δ and W . Thus, the tunneling in a DQD-based qubit would be affected by any fluctuations of Δ and W , both can lead to loss of coherency of the qubit. The ideal coherence is defined in a DQD where the probability for an electron to be in the left QD or in the right is about 1/2 for all possible states of the DQD. This qubit state corresponds to the limits $\Delta \rightarrow 0$ and $W > \Delta$; these occur in a range of $\Theta \sim 0$, where the relation $\tan(\Theta/2) \sim 1$ and the probability is close to 1/2. The limit $\Delta \rightarrow 0$ is a mathematical idealization, for which the spectral distribution of tunneling states in such ideal DQD corresponds to maximal coherence. However, the charge qubit initial state has to be weakly coupled and localized to realize binary logic. In this state, almost deal system is unstable relatively to small fluctuations. This conclusion flows down from the results of our calculations, where the numerical errors simulate the small variations of input parameters of the almost ideal DQD.

More realistic consideration is related to finite values of Δ . A simple case to mention is when $\Delta \neq 0$ may be induced by a geometrical asymmetry in DQD. The large Δ is appropriate to produce the initial state of a qubit as a localized state. To provide a large value for the ratio W/Δ and stable coherence, the value W has to be large so that $W > \Delta$ is always verified. Thus, there is apposite situation for the initial state (localized) and working state which must be delocalized.

The DQD-based charge qubit is stimulated by an electrical pulse⁷ which leads to tunneling (coherence) in DQD. For fabricated DQD, the energy difference Δ of the initial state is unrecoverable and this state can be a localized state, which might be

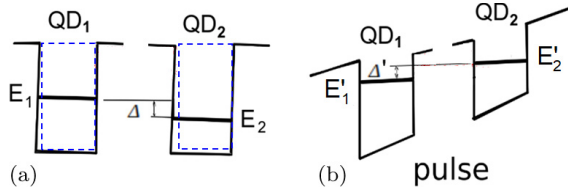


Fig. 9. (Color online) The confinement states (E_1 and E_2) of a single electron in separated QDs (QD₁ and QD₂): (a) without and (b) with an electrical pulse. The energy shift is $\Delta = E_2 - E_1$. Here, we assume that $\Delta' < \Delta$ is due to the bias of the confinement potential in the electrical field. The fine dashed contour demonstrates non-similarity of the QDs.

caused by, for example, a relatively large inter-dot distance (small W) and large value of the Δ . This realistic situation is schematically illustrated in Fig. 9; wherein (a) there is no tunneling and the separated QDs energy levels are shown. During the electrical pulse, the bias of the confinement potentials takes a place, as shown in Fig. 9(b) schematically. That makes a possibility for electron tunneling due to decreasing of the Δ and an increase of W due to the reduction of the depth of the quantum wells. In the last case, the corresponding energy levels become closer to the upper edge of the wells and the wave functions take more space around the centers of the QWs. We consider that the Δ' gets smaller than Δ . Thus, the large value for the ratio W/Δ is provided which means domination of the delocalized states and coherence in DQD. The coherence will be kept during the pulse. The form of the electric pulse can be found in Ref. 7. In this model, it is assumed that the fast pulse acts on the QDs in a non-adiabatic way.

We have seen that small Δ' increases the coherence in DQD. However, electrical field fluctuations during the pulse can give different causal values for Δ' . When $\Delta' \approx 0$, the effect of the fluctuation on the coherence may be large if the value of the W is enough small which means the coupling is weak. In other words, unstable tunneling in DQD corresponds to the case when $W \ll \Delta'$ according to Eq. (11). The tunneling will be stable when the W is relatively large $W \gg \Delta'$ which corresponds to strong coupling in DQD. Our next numerical simulation is dedicated to the relation between W and Δ .

We consider DQW with the asymmetry defined by the ratio $R_x/R_y = 15/14$ for semi-axes of right ellipsoidal shaped QW. The left QW has a spherical shape with a radius of 15 nm. The inter-dot distance was chosen as $a = 4$ nm to provide an electron localized state in the initial state. To simulate the electric pulse, we make an energy correction V_e for the effective potential V_c in the right QW so that $V'_c = V_c - V_e$. By increasing the value V_e , one can find the position of resonance tunneling when the electron state becomes delocalized. This position corresponds to the anti-crossing of the levels of a quasi-doublet. In Fig. 10, we present our results of the simulation. The dependence of the energy of the lowest quasi-doublet on the correction V_e demonstrates the anti-crossing in Fig. 10 (Upper panel). In the lower panel of the figure, we show the effect of the anti-crossing on the electron localization.

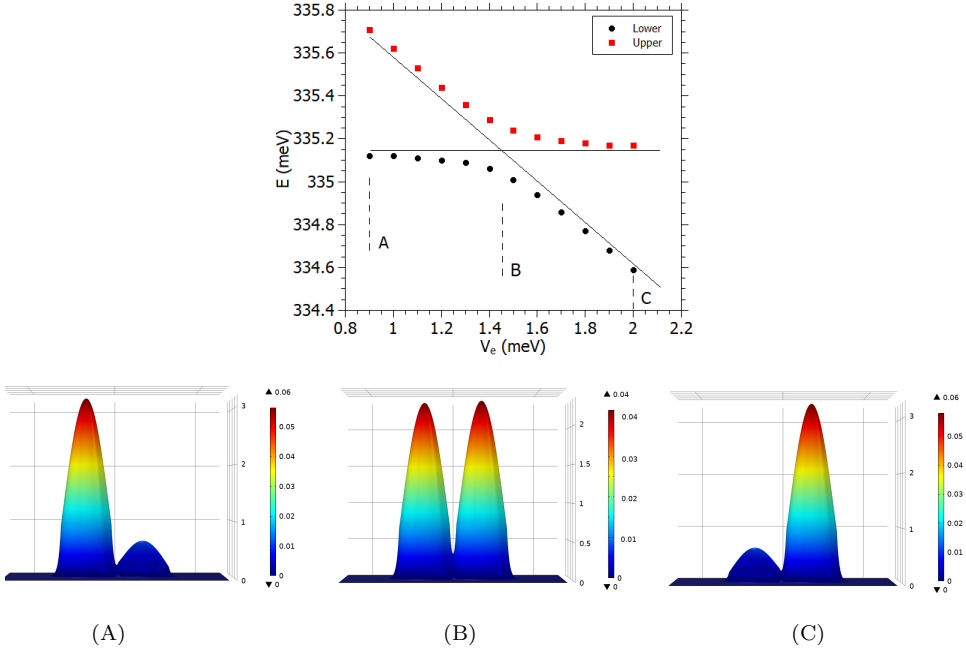


Fig. 10. (Color online) (Upper panel) The dependence of the energy of the lowest quasi-doublet on the energy correction V_e for the effective potential V_s in the right QW: $V'_s = V_s - V_e$. The considered DQW asymmetry defined by the semi-axes ratio R_x/R_y of right QW is 15/14. The inter-dot distance a was chosen to be 4 nm. The circular (square) dots show the results of calculation for lower member of the quasi-doublet (upper member). The solid lines show the imaginary cross of the levels. (Lower panel) The normalized cross-section of electron wave functions at the ground state in DQW for different V_e . The labels (A), (B) and (C) correspond to the V_e value in the upper panel (vertical dashed lines).

In the central point of anti-crossing, when $V_e = 1.45$ meV, the electron is delocalized with equal probability in both QWs. This probability becomes to asymmetric one when the V_e is going from the central value (point B). It looks like the electron change localization under the increasing of V_e from left QW (point A) to right QW (point C).

In our model for the charge qubit, the initial localized state is reached when the inter-dot distance a is equal to 4 nm and more. For shorter distances, the delocalization begins. We calculate the dependence of the electron localization on variations of a . The results are presented in Fig. 11, where the degree of the localization is expressed by the averaged x -coordinate and deviation of energy from averaged energy $E_{av} = (E_- + E_+)/2$. The electron states of the lowest spectral quasi-doublet are considered for the modeling. The result in Fig. 11(a) is interpreted as follows: the value of W rapidly decreases to zero, while Δ is large. This provides delocalized states for large distances. The energies E_- and E_+ approach to E_1 and E_2 , asymptotically. In Fig. 11(b), we show the results of the same calculations under the pulse simulated by $V_e = 1.45$ meV acting in the right QW. The electron state is delocalized one up to the value of 6 nm for the a . We can interpret Fig. 11 using the

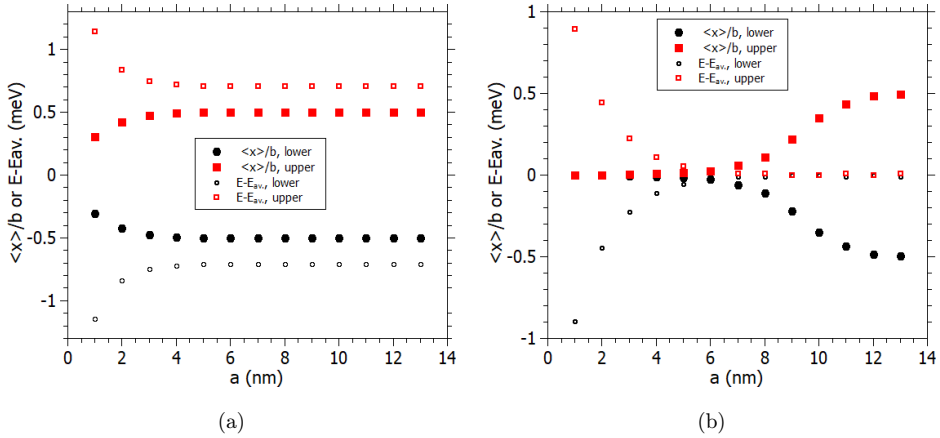


Fig. 11. (Color online) The averaged coordinate $\langle x \rangle/b$ (solid squares) and electron energy ($E - E_{av}$) (open squares) of lowest quasi-doublet for different values of the inter-dot distance a in an asymmetric DQW. The asymmetry of the DQW is defined by the ratio $R_x/R_y = 15/14$ for semi-axes of right QW. The calculation results are shown by different symbols. The values of a are given in the legend, b is normalizing constant: $b = a + 2R_x$. (a) $V_e = 0$. (b) $V_e = 1.45$ meV.

relation between W and Δ . In Fig. 11(a), at short distances when $a < 4$ nm, the W is large and quickly decreased. At the same time, the Δ is about zero. The ratio W/Δ is large and the electron is delocalized. For larger distances when $a > 6$ nm, the competition between W and Δ leads to localized states due to small W and $W \ll \Delta$, where Δ is small but finite. Our modeling for the electrical pulse gives stable coherence of the charge qubit due to increasing the ratio W/Δ , where W is initially weak coupling. This increase of tunneling is provided by decreasing Δ to small values of Δ' . However, as we have seen above in Eq. (11), the tunneling can be potentially unstable when $W \leq \Delta$ and $\Delta \approx 0$ since the sensitivity of tunneling on the Δ variations is proportional to $\frac{1}{\Delta}$.

Now, we can consider an almost ideal DQW to definite one more realization for a stable qubit. For example, we can remember the ion of H_2^+ where two identical protons are bound by an electron, interacting with the Coulomb potential. The idealization allows us to propose a stable qubit. The results of the corresponding calculations are presented in Fig. 12. Coherence in DQWs at large inter-dot distances is ensured by the similarity of QWs. We have illustrated this in Fig. 8. The averaged coordinate $\langle x \rangle/b$ (where $b = a + 2R_x$) is close to zero value and electron energies of the quasi-doublet are the same with the accuracy of 10^{-10} eV. That is the result of the numerical FEM approximation on the finite mesh. In Fig. 12(a), the correction V_e for V_s potential in the right QW (a pulse) leads to the loss of the almost ideal coherence. The quasi-doublet members are separated by energy and degree of localization due to large Δ . For short inter-dot distance a , Δ is comparable with W and we see a partial delocalization. When a is large, the relation $W \ll \Delta$ is satisfied and the electron states are localized. It can be an initial state of the qubit. The coherence state

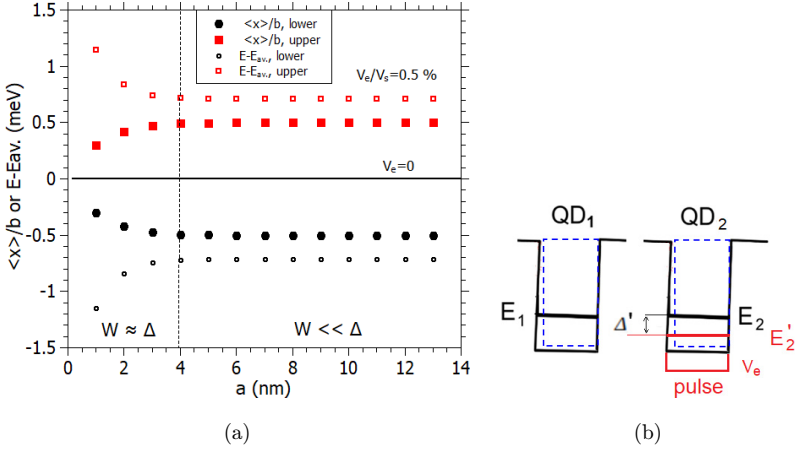


Fig. 12. (Color online) (a) The averaged coordinate $\langle x \rangle/b$ (solid squares) and electron energy $(E - E_{av.})$ (open squares) of lowest quasi-doublet for different values of the inter-dot distance a in almost ideal DQW. The radii of the circle-shaped QWs are 15 nm. The asymmetry of the DQW is induced by geometry approximation inherent to FEM, since the mesh finesse is limited ($\Delta < 10^{-10}$ eV). The V_s potential is corrected by $V_e = 1.45$ meV in the right QW, and the horizontal line corresponds to the results obtained with $V_e = 0$. The remaining notations are the same as those used in Fig. 11. The dashed vertical line separated two regions where $W \approx \Delta$ and $W \ll \Delta$. (b) The schematics diagram for the qubit based on the almost ideal DQD. The electrical pulse (pulse) changes the confinement (in red color) in the right QD so that the energy level E_2 is shifted by the value Δ' where $\Delta' \gg \Delta$. The small Δ is not shown. The fine dashed contour demonstrates an arbitrary geometry for these similar QDs.

is produced when the correction V_e is switched off. The graphical description of the model is shown in Fig. 12(b).

For practical realization, the QW must be almost identical. This is the hard problem of fabrication. The future modeling including different materials can allow approaching to almost ideal DQW. For example, the shallow electron confinement leads to a large value W that forced the coupling and make a weaker condition for the similarity of QWs. The same effect is obtained by decreasing the size of QWs. The results of such calculations are presented in Fig. 13. We reduced the radii of QWs to 5 nm. The inter-dot distance was chosen to be 4 nm. The asymmetry of the DQW is simulated by decreasing the semi-axes of right QW $R'_y = R_y - \kappa/100$, where the parameter κ is increased from zero value. The initial state $\kappa = 0$ is delocalized one with the probability of 1/2 for an electron to be in the left or the right QW. Increasing κ leads to the breaking of the ideal coherence. However, this breaking is not significant up to $\kappa \approx 5$ nm. In this region, the relation $W > \Delta$ has to take place. A more strong violation of the geometry symmetry leads to increasing of Δ and decreasing W . So that the relation $W < \Delta$ is satisfied. The state of an electron becomes to localized one when $\kappa > 30$ nm. Thus, the DQW keeps a coherence with asymmetry up to 5%. We can increase this limit by increasing the coupling W . It can be done for example by reducing the size, topology or material composition of the QWs.

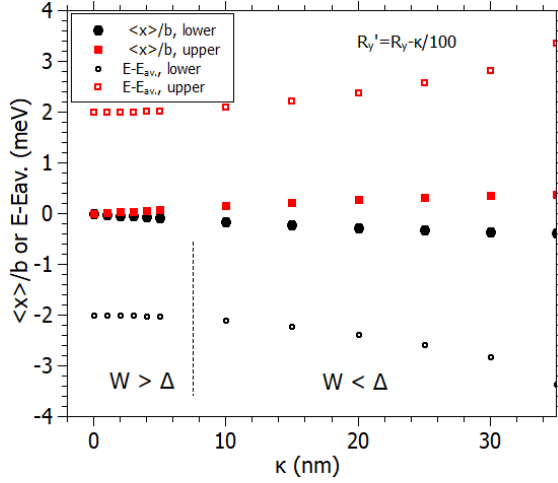


Fig. 13. (Color online) The effect of geometry asymmetry in almost ideal DQW. The radii of the circle shaped QWs are 5 nm. The asymmetry of the DQW is simulated by decreasing the semi-axes of right QW: $R'_y = R_y - \kappa/100$ where the parameter κ is varied. Other notations are similar to the ones used in previous figure. The dashed vertical line separates the region where $W > \Delta$ from that where $W < \Delta$.

The environmental induced fluctuations are mainly related to W . The environment media interacting with the electron in DQD distorts the wave functions and changes the matrix elements W . The complex competition of the two factors Δ and W reduced to the dependence of the coherence on W . We have seen that for different symmetries of wave functions of different spectral states produce clear picture of the W influence on the tunneling in DQW. An essential decreasing of W leads to lost of the coherence.

The effects of the environmental fluctuations of the pulse in the charge qubit have been formalized in Refs. 35–37, where the dephasing of a superconductor qubit was investigated. The wave function taking into account the dephasing can be represented by the formula: $|0\rangle + \beta e^{i\phi(t)}|1\rangle$, where the pre-factor of the $e^{i\phi(t)}$ phase term can be described by a Gaussian distribution that expresses the fluctuations. Our analysis is in agreement with this phenomenological formalization.

7. Conclusions

The localization of a single electron in 2D binary quantum systems was numerically studied using the effective potential model for InAs/GaAs nano-sized heterostructure. The emphasis was on the differences between the system elements (subsystems). The effect related to the breaking of similarity of the subsystems has been discussed. Prior considerations of such systems were limited to symmetrical shapes of identical QDs.

The variation of similarities was controlled and symmetrical versus asymmetrical shapes of QWs within DQW were studied. To that end, the energy of confinement states $E^{(n)}$, $n = 0, 1, \dots$, and the spatial localization of a single electron, detected by averaged coordinate x of the electron the DQW, were calculated. The effect of symmetry breaking on localization is explained in terms of the theory of two-level systems. To explain our results, an elementary introduction to the theory was provided. Two key parameters that affect the electron localization were identified; the first one, W_n , is the overlap of the wave functions of separated QWs, and the second one, Δ_n , is the energy difference for n th electron levels in the spectra of the separated QDs.

We showed that the ratio W_n/Δ_n determines the spectral distribution of the localized/delocalized states in DQW. The concurrent effects of $W^{(n)}$ and $\Delta^{(n)}$ on the electron localization are shown by variations of the DQD geometry. We can conclude that the spectral distribution of the electron tunneling demonstrates high sensitivity to the DQW geometry variations.

We considered the strong and weak coupling of QWs. These are delineated through relation between W and Δ : $W > \Delta$ for the strong coupling, and $\Delta \approx 0$, $W < \Delta$ for the weak coupling. In particular, we showed for an ideal DQW that the electron coupling of QWs can be unstable for any small violation of the symmetry, even when $\Delta \rightarrow 0$. As example of weak coupling in the ideal DQW, we have presented numerical calculations with variable finite element meshes. The set of meshes generates variations of the Δ . The corresponding distributions of localized/delocalized states demonstrate unstable tunneling for relatively small variations of Δ . At the same time, the coherence in ideal DQW was found to be independent of the inter-dot distance.

Our approach based on a study of localized/delocalized states in DQW can be used for study of limitations for the stability of charge qubits. We simulated a charge qubit in which the effect of the electrical field is used to ensure the coherence of the qubit. The relation between W and Δ in establishing the qubit coherence was shown. The decreasing of the value of Δ under the pulse gives stable coherence. Based on our modeling, the fluctuations of electric pulse can result in variations of the energy shift Δ . It must also be noted that establishing strong coupling is important due to the environmental fluctuations impact the symmetry of bi-confinement in the DQW and can result in fluctuations of overlapping integral W that led to loss of coherence.


Ultimately one should consider a qubit, based on almost ideal DQW. As a means for controlling the qubit, and its coherence, one can use pulses of other nature than electric pulses. The pulse can generate binary logic. The coherence is established due to the almost ideal property of this DQW and a pulse will not be needed. However, the problem of environmental influence remains has to be addressed in a different way.


Acknowledgments


This work is supported by the National Nuclear Security Administration award NA0003979, and the US National Science Foundation, EIR 2101041, DMR-2101220, DMR-2101041, and HRD-1345219 awards, and DHS Award 23STSLA00015.


S.P.K. would like to thank the Leibniz Foundation of the University of Leipzig for their support and hospitality during his visit.

ORCID

Igor Filikhin  <https://orcid.org/0000-0003-0046-2902>

Abdennaceur Karoui  <https://orcid.org/0000-0003-2028-8737>

Sergei P. Kruchinin  <https://orcid.org/0000-0002-0674-5826>

Branislav Vlahovic  <https://orcid.org/0000-0001-8965-1480>

References

1. D. Loss and D. P. DiVincenzo, *Phys. Rev. A* **57** (1998) 120.
2. J. M. Elzerman, R. Hanson, J. S. Greidanus, L. H. W. van Beveren, S. De Franceschi, L. M. K. Vandersypen, S. Tarucha and L. P. Kouwenhoven, *Phys. Rev. B* **67** (2003) 161308.
3. M. Ciorga, A. S. Sachrajda, P. Hawrylak, C. Gould, P. Zawadzki, S. Jullian, Y. Feng and Z. Wasilewski, *Phys. Rev. B* **61** (2000) R16315.
4. F. H. L. Koppens, C. Buizert, K. J. Tielrooij, I. T. Vink, K. C. Nowack, T. Meunier, L. P. Kouwenhoven and L. M. K. Vandersypen, *Nature* **442** (2006) 766.
5. J. R. Petta, A. C. Johnson, C. M. Marcus, M. P. Hanson and A. C. Gossard, *Phys. Rev. Lett.* **93** (2004) 186802.
6. T. H. Oosterkamp, T. Fujisawa, W. G. van der Wiel, K. Ishibashi, R. V. Hijman, S. Tarucha and L. P. Kouwenhoven, *Nature* **395** (1998) 873.
7. J. Gorman, D. G. Hasko and D. A. Williams, *Phys. Rev. Lett.* **95** (2005) 090502.
8. C. B. Simmons et al., *Nano Lett.* **9** (2009) 3230.
9. S. D. Sarma, X. Wang and S. Yang, *Phys. Rev. B* **83** (2011) 235314.
10. R. Taranko and T. Kwapiński, *Physica E* **48** (2013) 157.
11. M. Raith, C. Ertler, P. Stano, M. Wimmer and J. Fabian, *Phys. Rev. B* **89** (2014) 085414.
12. T. Hayashi, T. Fujisawa, H. D. Cheong, Y. H. Jeong and Y. Hirayama, *Phys. Rev. Lett.* **91** (2003) 226804.
13. X. Wang, S. Yang and S. D. Sarma, *Phys. Rev. B* **84** (2011) 115301.
14. L. Pan, X. Wang, X. Cui and S. Chen, *Phys. Rev. A* **102** (2020) 023306.
15. Y. Zheng and S. Yang, *Phys. Rev. A* **104** (2021) 023304.
16. I. Filikhin, V. M. Suslov and B. Vlahovic, *Phys. Rev. B* **73** (2006) 205332.
17. I. Filikhin, A. Karoui and B. Vlahovic, *J. Nanotechnol.* **2016** (2016) 3794109.
18. I. Filikhin, S. G. Matinyan and B. Vlahovic, *Quantum Matter* **3** (2014) 549.
19. I. Filikhin, S. G. Matinyan and B. Vlahovic, *Sensors Transducers* **183** (2014) 116.
20. I. Filikhin, A. Karoui and B. Vlahovic, *Int. J. Mod. Phys. B* **30** (2016) 1642011.
21. D. J. BenDaniel and C. B. Duke, *Phys. Rev.* **152** (1966) 683.
22. A. Schliwa, M. Winkelkemper and D. Bimberg, *Phys. Rev. B* **76** (2007) 205324.
23. I. Filikhin, T. Peterson, B. Vlahovic, S. P. Kruchinin, Y. B. Kuzmichev and V. Mitic, *Physica E* **114** (2019) 113626.
24. A. Lorke, R. J. Luyken, A. O. Govorov, J. P. Kotthaus, J. M. Garcia and P. M. Petroff, *Phys. Rev. Lett.* **84** (2000) 2223.

25. I. Filikhin, V. M. Suslov and B. Vlahovic, *J. Comput. Theor. Nanosci.* **9** (2012) 669.
26. W. Lei, C. Notthoff, A. Lorke, D. Reuter and A. D. Wieck, *Appl. Phys. Lett.* **96** (2010) 033111.
27. C. Cohen-Tannoudji, B. Diu and F. Laloe, *Quantum Mechanics*, Vol. **1** (Wiley-VCH, Germany, 1977).
28. J. A. C. Johnson, C. M. Marcus, M. P. Hanson and A. C. Gossard, *Phys. Rev. B* **71** (2005) 115333.
29. Z. M. Wang, K. Holmes, Y. I. Mazur, K. A. Ramsey and G. J. Salamo, *Nanoscale Res. Lett.* **1** (2006) 57.
30. C.-P. Yang, S.-I. Chu and S. Han, *Phys. Rev. A* **67** (2003) 042311.
31. M. H. S. Amin, A. Y. Smirnov and A. M. van den Brink, *Phys. Rev. B* **67** (2003) 100508.
32. K. Nomoto, R. Ugajin, T. Suzuki and I. Hase, *J. Appl. Phys.* **79** (1996) 291.
33. T. Tanamoto, *Phys. Rev. A* **61** (2000) 022305.
34. L. Fedichkin, M. Yanchenko and K. A. Valiev, *Nanotechnology* **11** (2000) 387.
35. J. M. Martinis, S. Nam, J. Aumentado, K. M. Lang and C. Urbina, *Phys. Rev. B* **67** (2003) 094510.
36. F. Yoshihara, K. Harrabi, A. O. Niskanen, Y. Nakamura and J. S. Tsai, *Phys. Rev. Lett.* **97** (2006) 167001.
37. L. Cywiński, R. M. Lutchyn, C. P. Nave and S. D. Sarma, *Phys. Rev. B* **77** (2008) 174509.